

## Magmatic evolution of impact-induced Martian mantle plumes and the origin of Tharsis

C. C. Reese,<sup>1</sup> V. S. Solomatov,<sup>2</sup> J. R. Baumgardner,<sup>3</sup> D. R. Stegman,<sup>4</sup> and A. V. Veizolainen<sup>2</sup>

Received 5 December 2003; revised 27 May 2004; accepted 21 June 2004; published 31 August 2004.

[1] Tharsis province is a major center of Martian volcanic activity characterized by large gravity and topography anomalies. The origin of Tharsis is debated. One hypothesis is that the province was produced by melting associated with a mantle plume from the core-mantle boundary. An alternative hypothesis is that Tharsis formed by a plume associated with an impact. Recent studies have shown that this hypothesis is plausible from a geodynamical point of view and that long-lived impact plumes might play a role in areoid evolution. In this study, the magmatic evolution of impact-induced thermochemical mantle plumes is investigated with fully three-dimensional spherical shell simulations of mantle convection. Melt volumes and emplacement rates predicted by the model can satisfy observational constraints on Tharsis development. *INDEX TERMS:* 6225 Planetology: Solar System Objects: Mars; 5430 Planetology: Solid Surface Planets: Interiors (8147); 5455 Planetology: Solid Surface Planets: Origin and evolution; 8121 Tectonophysics: Dynamics, convection currents and mantle plumes; *KEYWORDS:* impact plumes, mantle dynamics, Mars

**Citation:** Reese, C. C., V. S. Solomatov, J. R. Baumgardner, D. R. Stegman, and A. V. Veizolainen (2004), Magmatic evolution of impact-induced Martian mantle plumes and the origin of Tharsis, *J. Geophys. Res.*, 109, E08009, doi:10.1029/2003JE002222.

### 1. Introduction

[2] Tharsis is one of the most prominent features on Mars. Volcanism and tectonism associated with the plateau by far exceed the levels of activity in other areas of the planet. This monopolar distribution of tectonism and volcanism led to the suggestion that the planform of mantle convection on Mars is dominated by a single, long-lived, thermal plume originating at the core-mantle boundary similar to a terrestrial plume but much larger [Hartmann, 1973; Carr, 1974; Phillips and Ivins, 1979]. Deep mantle mineralogical phase transformations are capable of stabilizing a one-plume pattern of convection [Weinstein, 1995; Harder and Christensen, 1996; Breuer et al., 1998; Spohn et al., 1998; Harder, 2000].

[3] Although the conventional plume model explains some features of Tharsis, there are both observational and theoretical reasons to consider alternatives. First, the plume model has not reproduced Tharsis development on time-scales consistent with observations [Banerdt and Golombek, 2000; Phillips et al., 2001; Johnson and Phillips, 2003; Zuber, 2001]. Second, the plume model only accounts for dynamic support of Tharsis. Crustal thickening [Zuber et

al., 2000] and observations of layered sequences of rock in the walls of Valles Marineris [McEwen et al., 1999] suggest that constructional volcanism is a major contributor to Tharsis elevation [Solomon and Head, 1982]. Also, a recent analysis suggests that Tharsis is predominantly supported by crustal thickening and lithospheric flexure while a thermal plume would contribute only a fraction to the present-day topography and areoid [Zhong, 2002; Lowry and Zhong, 2003; Zhong and Roberts, 2003]. Third, the plume hypothesis implies an actively convecting mantle and a sufficiently large heat flux from the Martian core. However, in the absence of plate tectonics, Martian mantle convection can be very sluggish [Grasset and Parmentier, 1998; Reese et al., 1998, 2002; Solomatov and Moresi, 2000]. Scaling relationships [Solomatov and Moresi, 2000] for olivine rheology [Karato and Wu, 1993] indicate that a wet mantle convects only in a narrow subsolidus temperature range while a dry mantle is convectively stable even above melting temperatures. A pyroxene rich Martian mantle [Bertka and Fei, 1998a, 1998b, 1999; Sanloup et al., 1999] can be relatively viscous compared to an olivine rich mantle [Ave Lallemand, 1978; Ross and Nielsen, 1978; Mackwell, 1991] making initiation of convection at subsolidus temperatures even more difficult [Reese et al., 2002]. Widespread melting would, in turn, differentiate heat producing elements [Turcotte, 1989; Spohn, 1991; Schubert et al., 1992], increase viscosity [Karato, 1986], and produce compositional stratification all of which tend to suppress convection. It seems that in the stagnant lid regime, vigorous Martian mantle convection is difficult to initiate and maintain.

[4] In addition, rapid development of a conventional thermal plume at the core-mantle boundary after planetary

<sup>1</sup>Division of Science and Mathematics, University of Minnesota, Morris, Morris, Minnesota, USA.

<sup>2</sup>Department of Physics, New Mexico State University, Las Cruces, New Mexico, USA.

<sup>3</sup>Theoretical Division, Los Alamos National Laboratory, Los Alamos, New Mexico, USA.

<sup>4</sup>Department of Earth and Planetary Science, University of California, Berkeley, Berkeley, California, USA.

formation could be problematic because of mantle heating. Although a transient episode of early surface recycling [Sleep, 1994] can facilitate mantle cooling, the duration might be short [Tajika and Sasaki, 1996] and the subsequent transition to stagnant lid convection would result in mantle heating shutting off any core heat flux and associated plume activity [Nimmo and Stevenson, 2000]. The liquid state of the Martian core recently inferred from solar tidal deformation is consistent with such a possibility [Yoder et al., 2003].

[5] Isotopic evidence also argues against vigorous mantle mixing. SNC meteorite Hf/W and Sm/Nd systematics suggest that core and crust formation were contemporaneous and occurred within  $\sim 30$  Myr of planet formation [Harper et al., 1995; Lee and Halliday, 1997; Halliday et al., 2001]. Survival of isotopic heterogeneity in the Martian upper mantle since the time of core formation and early vigorous convection are difficult to reconcile [Zuber, 2001]. Large variations in Sm/Nd and Lu/Hf ratios among shergottites also suggest a heterogeneous mantle which retains an isotopic signature of initial differentiation [Albarède et al., 2000]. Finally, cessation of Xe degassing early in Mars history suggests that large scale mantle magmatism, and presumably vigorous convection, have been limited since 300 Myr [Marty and Marti, 2002] after formation.

[6] An alternative hypothesis is that Tharsis could be associated with a large impact early in Martian history [Schultz and Glicken, 1979; Schultz, 1984; Schultz and Frey, 1990]. Geodynamical consequences of this hypothesis were investigated by Reese et al. [2002]. The authors demonstrate that impact-induced thermal plumes can survive for the entirety of planetary evolution and play a role in areoid evolution.

[7] Additional constraints are provided by the magmatic evolution of Tharsis. In this study, the impact plume hypothesis for the origin of Tharsis is investigated further by calculating the spatial and temporal distribution of decompression melt resulting from upwelling of an initially shock-melted region which is buoyant due to mantle depletion, melt retention, and shock heating. Enhanced near surface melting due to decompression associated with opening of the transient crater [Jones et al., 2002; Elkins-Tanton et al., 2002] is debated [Melosh, 2000] and is neglected in this study. It is assumed that mantle melt is extracted and transferred toward the surface resulting in intrusive and extrusive magmatism. Permanent structural uplift of an upper mantle magmatic system and development of Tharsis was discussed by Phillips et al. [1990]. Production of Tharsis by an impact-related plume requires neither globally occurring convection nor generation of plumes at the core-mantle boundary.

## 2. Model

### 2.1. Initial Conditions

[8] Large impacts at the end of planetary formation are a statistically inevitable consequence of accretional dynamics [Wetherill, 1985, 1990; Weidenschilling et al., 1997; Chambers and Wetherill, 1998; Agnor et al., 1999]. Impacts with  $\sim 0.1$  impactor/planet mass ratio are sufficiently energetic to melt a region with radius on the order of several impactor radii [Melosh, 1990; Tonks and Melosh, 1992, 1993; Pierazzo et al., 1997].

[9] The three major processes following the impact are crystallization, isostatic adjustment and melt percolation. Melt distribution in the impact heated region varies strongly, from superliquidus conditions near the surface to subsolidus conditions deeper in the mantle. Cooling and crystallization of regions with the highest degree of melting to about 60% crystal fraction can be very fast, on the scale of  $10^3$  years [Solomatov, 2000].

[10] Isostatic adjustment of the region with melt fraction varying from 40% to 0% is slower. Although the geometry of the melt region and density distribution is rather complex, the time scale for isostatic adjustment can be estimated as

$$t_{\text{iso}} \sim \frac{\pi \eta}{\Delta \rho_{\text{iso}} g R}, \quad (1)$$

where  $\eta$  is the mantle viscosity,  $R$  is the radius of the hemispherical molten region, and  $\Delta \rho_{\text{iso}}$  is the driving density difference between the surrounding mantle and molten region. The coefficient  $\pi$  is taken from the problem of isostatic adjustment of a sinusoidal perturbation (wavelength  $\lambda = 4R$ ) of the interface between two half spaces with the density difference  $\Delta \rho$  (see, for example, the classical postglacial rebound problem [Turcotte and Schubert, 2002]). The only modification necessary is to replace the driving density  $\Delta \rho$  by  $\Delta \rho_{\text{iso}}$ . A similar coefficient can be obtained for the time scale required for an inviscid sphere of radius  $R$  with the density difference  $\Delta \rho_{\text{iso}}$  to travel the distance  $R$ . With  $\eta \approx 10^{22}$  Pa s,  $\Delta \rho_{\text{iso}}/\rho \approx 0.02$  (for the entire region heated by impact),  $\rho = 3300$  kg m $^{-3}$ ,  $g = 3.7$  m s $^{-2}$  and  $R \approx 10^6$  m, the isostatic adjustment time  $t_{\text{iso}} \approx 4 \cdot 10^6$  years. Melt percolation through a partially crystallized matrix is a much slower process which can take more than  $10^8$  years [Solomatov, 2000] (see also estimates below).

[11] Thus a qualitative description of the entire process is as follows. A very fast initial crystallization produces a region with melt fraction varying from about 40% near the surface to 0% several hundred kilometers below the surface. Because of its positive buoyancy, this region floats up. Hot, partially molten material rises and spreads out on the surface of the planet and is replaced by colder, less molten material from below. All processes slow down as the melt fraction and driving density difference decrease and the viscosity increases. At some point, the dynamics becomes sufficiently slow such that the problem can be addressed numerically with the goal of capturing some important features of the subsequent evolution of the planet.

[12] Initial conditions for the calculations are generated as follows. The average, preimpact, mantle temperature is assumed to be 1800 K with fixed surface temperature of 220 K (Figure 1). The impact heated region produced by the shock wave due to a nearly vertically incident impactor has been modeled analytically as a hemisphere or truncated sphere [Tonks and Melosh, 1992, 1993] with numerical experiments supporting the latter geometry [Pierazzo et al., 1997]. Highly oblique impacts concentrate energy downrange at shallower depths [Pierazzo and Melosh, 2000]. Early dynamic processes undoubtedly modify this simple geometry. For the purposes of this study, the region left heated after impact shock melting and fast initial crystallization is assumed to be hemispherical with radius  $R$  left as a model parameter related to impactor size and

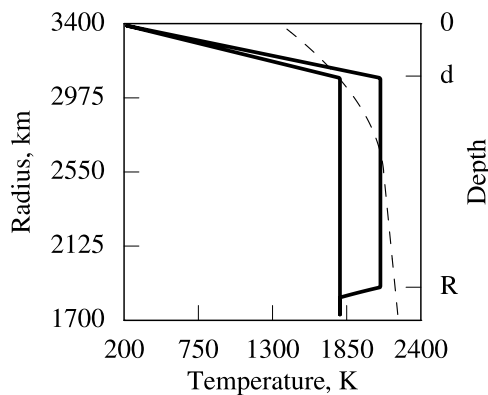


**Figure 1.** Average preimpact mantle temperature and postimpact/crystallization temperature profile on axis of the hemispherical region with radius  $R$  (solid lines). Peridotite solidus is shown with a dashed line. Nominal mantle temperature is 1800 K, and the initial cold boundary layer thickness is  $d \sim 300$  km, implying subsolidus mantle conditions. The temperature increase within the anomaly is 300 K. Upper mantle supersolidus temperatures are dropped immediately to the melting curve (see text). The profile shown is for  $R = 1500$  km.

velocity (see Discussion). The thermal anomaly is assumed to be uniform with  $\Delta T = 300$  K (Figure 1). Because any core heat flux was probably short lived [Nimmo and Stevenson, 2000], the bottom boundary is assumed to be insulating throughout evolution. The initial cold boundary layer thickness is resolution limited to  $\sim 300$  km.

## 2.2. Melting

[13] Mantle solidus temperature is parameterized according to experimental data for peridotite [Scarfe and Takahashi, 1986; Ito and Takahashi, 1987; McKenzie and Bickle, 1988; Herzberg and Zhang, 1994]

$$T_m = 1374 + 130p - 5.6p^2, \quad (2)$$

where  $T_m$  is in Kelvin and pressure in gigapascals. After the slope reaches  $dT_m/dp = 10$  K/GPa $^{-1}$ , solidus temperature increases linearly with pressure. Only dry melting below 8 GPa is considered.

## 2.3. Depletion/Retained Melt Buoyancy

[14] The density of the material undergoing melting is affected by both the composition change of the residual mantle and the retained melt fraction. Preferential melting of dense mineral phases results in a decrease of residual mantle density and an associated compositional buoyancy. The mantle residuum density depends on mantle composition, mineralogy and melt fraction. It drops by approximately 1% for every 10% of melt extraction [e.g., Oxburgh and Parmentier, 1977; Sparks and Parmentier, 1993; Raddick et al., 2002].

[15] Since it takes time for melt to escape, some melt fraction will be present after the material has undergone partial melting. The amount of melt present in the mantle depends on how much melt has been generated and how quickly it escapes from the matrix. The melt fraction generated in the upwelling is determined by the depth at

which the temperature in the adiabatic upwelling reaches the solidus and the depth where the upwelling stops (basically the bottom of the lid). In our simulations the melt fraction in this melt channel at the top of the upwelling reaches about 10%. The density reduction caused by the presence of 10% melt is about  $\phi\Delta\rho/\rho_{\text{solid}} \sim 1.5\%$ , where  $\phi$  is the melt fraction,  $\rho_{\text{solid}} \approx 3300$  kg m $^{-3}$  is the density of the solid matrix, and  $\Delta\rho \approx 500$  kg m $^{-3}$  is the density difference between the matrix and the melt.

[16] How much of this melt escapes from the matrix depends on the melt viscosity. The viscosity of basaltic melts can be very high, exceeding 100 Pa s [Kushiro, 1980, 1986]. It depends strongly on the composition and, in particular, on the silica content which affects the degree of polymerization. Viscosities over  $10^4$  Pa s have been estimated for basaltic lavas on Mars [Warner and Gregg, 2003] although this value might be affected by the presence of phenocrysts and bubbles.

[17] The melt fraction left in the partially molten region can be estimated from the requirement that melt cannot escape on the time scale of convective flow through the melting region. This is equivalent to the requirement that the characteristic convective velocity  $u_{\text{conv}}$  is comparable to the percolation velocity  $u_{\text{perc}}$ :

$$u_{\text{conv}} \sim u_{\text{perc}}. \quad (3)$$

[18] The percolation velocity of melt through the solid matrix can be estimated using the Ergun-Orning formula [Soo, 1967; Dullien, 1979]:

$$u_{\text{perc}} = \frac{g\Delta\rho d^2 \phi^2}{150\eta_{\text{melt}}(1-\phi)}, \quad (4)$$

where  $d$  is the grain size.

[19] The above equations give an estimate for the retained melt fraction:

$$\begin{aligned} \phi &\sim \left( \frac{150\eta_{\text{melt}}u_{\text{conv}}}{g\Delta\rho d^2} \right)^{1/2} \\ &\sim 0.03 \left( \frac{\eta_{\text{melt}}}{100 \text{ Pa s}} \right)^{1/2} \left( \frac{u_{\text{conv}}}{0.3 \text{ cm/year}} \right)^{1/2} \left( \frac{10^{-3} \text{ m}}{d} \right). \end{aligned} \quad (5)$$

The density reduction corresponding to 3% melt is about 0.5%. On the other hand, if the melt viscosity is lower (say by about one order of magnitude), practically all the melt could be carried through the melting zone and will gradually escape later.

[20] Since the model does not actually calculate two-phase flow and variations of melt fraction in space and time are not considered, the combined effects of the compositional change and the presence of melt are accounted for by simply assuming that the fractional density difference  $\beta$  between mantle which has undergone melting and unmelted mantle is a constant  $\beta = 0.02$ . For the parameter values given above, this value corresponds to  $\sim 15\%$  melt extraction and  $\sim 3\%$  melt retention.

## 2.4. Internal Heating

[21] Stagnant lid scaling relationships suggest early, widespread mantle melting and possible extensive differen-

**Table 1.** Mars Parameters

Parameter	Notation	Value
Planet radius	$r_p$	3389 km
Core radius	$r_c$	1726 km
Thermal conductivity	$k$	4 W/m K
Thermal expansion	$\alpha$	$2 \times 10^{-5} \text{ K}^{-1}$
Reference density	$\rho$	$3470 \text{ kg m}^{-3}$
Compositional buoyancy parameter	$\beta$	0.02
Gravitational acceleration	$g$	$3.7 \text{ m s}^{-2}$
Specific heat capacity	$c_p$	$1200 \text{ J kg}^{-1} \text{ K}^{-1}$
Surface temperature	$T_s$	220 K
Initial mantle temperature	$T_0$	1800 K
Latent heat of fusion	$L$	$500 \text{ kJ kg}^{-1}$

tiation of heat producing elements into the crust [Reese et al., 1998, 2002; Hauck and Phillips, 2002]. Geochemical analysis also suggests early separation of a radiogenic isotope enriched crust [McLennan, 2001]. An end-member model of complete mantle differentiation is considered, i.e., there is no internal heating.

### 2.5. Viscosity

[22] An exponential viscosity law is used,

$$\eta = b \exp(-\gamma T), \quad (6)$$

where  $b$  and  $\gamma$  are constant. At large viscosity contrasts, the differences between Arrhenius [Karato and Wu, 1993] and exponential laws are unimportant for determining the interior temperature [Reese et al., 1999a]. A rigid upper surface, spherically averaged viscosity contrast  $\Delta\eta \sim 10^3$ , and maximum  $\Delta\eta \sim 3 \times 10^3$  ensure stagnant lid convection [Dumoulin et al., 1999; Solomatov and Moresi, 2000]. The interior mantle viscosity is left as a free parameter.

### 2.6. Convection Equations and Numerical Method

[23] The hydrodynamic equations expressing conservation of mass, momentum, and energy in the Boussinesq approximation and large Prandtl number limit are

$$\frac{\partial u_i}{\partial x_i} = 0, \quad (7)$$

$$\frac{\partial \tau_{ij}}{\partial x_j} = -\frac{\partial p}{\partial x_i} + \rho g_i, \quad (8)$$

$$\rho c_p \left( \frac{\partial T}{\partial t} + u_i \frac{\partial T}{\partial x_i} \right) = k \frac{\partial^2 T}{\partial x_i \partial x_i} - \rho L \frac{\partial f}{\partial t}, \quad (9)$$

where  $x_i$  are the spatial coordinates,  $t$  is the time,  $u_i$  is the velocity,  $p$  is the dynamic pressure,  $T$  is the temperature,  $c_p$  is the specific heat at constant pressure,  $k$  is the thermal conductivity,  $L$  is the latent heat of fusion, and  $f$  is the melt fraction. The deviatoric stress tensor

$$\tau_{ij} = \eta \left( \frac{\partial u_i}{\partial x_j} + \frac{\partial u_j}{\partial x_i} \right). \quad (10)$$

The density

$$\rho = \rho_0 [1 - \alpha(T - T_0) - \xi\beta], \quad (11)$$

where  $\rho_0$  is the reference density at reference temperature  $T_0$ ,  $\beta = 0.02$  is the buoyancy parameter, and  $\xi$  is a variable equal to 1 for material which has undergone any degree of partial melting and 0 otherwise (see section 2.3). While melt retention and depletion buoyancy drive mantle flow, changes in volume upon melting are neglected (i.e., a strict Boussinesq approximation is adopted).

[24] The fully three-dimensional spherical shell code TERRA [Baumgardner, 1985; Bunge and Baumgardner, 1995; Reese et al., 1999b] is used to study evolution of impact-induced thermal and compositional heterogeneity. Compositional information, i.e., the variable  $\xi$ , is carried by particles in the material reference frame which are advected according to the velocity field. The particle compositional field is interpolated back onto the finite element mesh allowing interaction with the flow via equation (11). Thus for a finite volume,  $\xi$  is the volume fraction which has undergone partial melting.

[25] The melt fraction [Hess, 1992]

$$f = \frac{c_p}{L} (T - T_m). \quad (12)$$

Model parameters (Table 1) imply a melting rate of  $\sim 0.2\%/K$  above solidus. Mantle melting near solidus is nearly eutectic in which case the temperature is not far from the solidus and the melting rate is not very different than that suggested by more sophisticated models [e.g., McKenzie and Bickle, 1988, 1990]. Degree of depletion and melt composition are not accounted for in the melting model. Melt is assumed to be immediately extracted from the mantle producing intrusive and extrusive magmatism. This material is not addressed by the model.

[26] Initial supersolidus temperatures at pressures  $\leq 8$  GPa are dropped immediately to the melting curve (Figure 1). While this material is assumed to be compositionally buoyant due to impact heating, melting and differentiation, this initial melt is not included in the calculation of the total melt volume. In this sense, the melt volume calculated in the model only represents that associated with upwelling material which intersects the solidus from below.

## 3. Results

[27] Compositional buoyancy associated with impact-induced heating, melting, and differentiation produces a localized mantle upwelling: an impact-induced plume. The upwelling velocity decays with time from an initial maximum that scales inversely with interior viscosity. Subsequent to the initial compositionally driven flow, evolution depends on interior viscosity. For high interior viscosity ( $\eta_i \geq 10^{22}$  Pa s), the thermal evolution is dominated by conduction. The stagnant lid thickens conductively but remains convectively stable. Interior velocities are very low and approximately constant throughout evolution. For low interior viscosity ( $\eta_i \leq 10^{21}$  Pa s), lid thickening leads to development of small scale instabilities at the lid base.

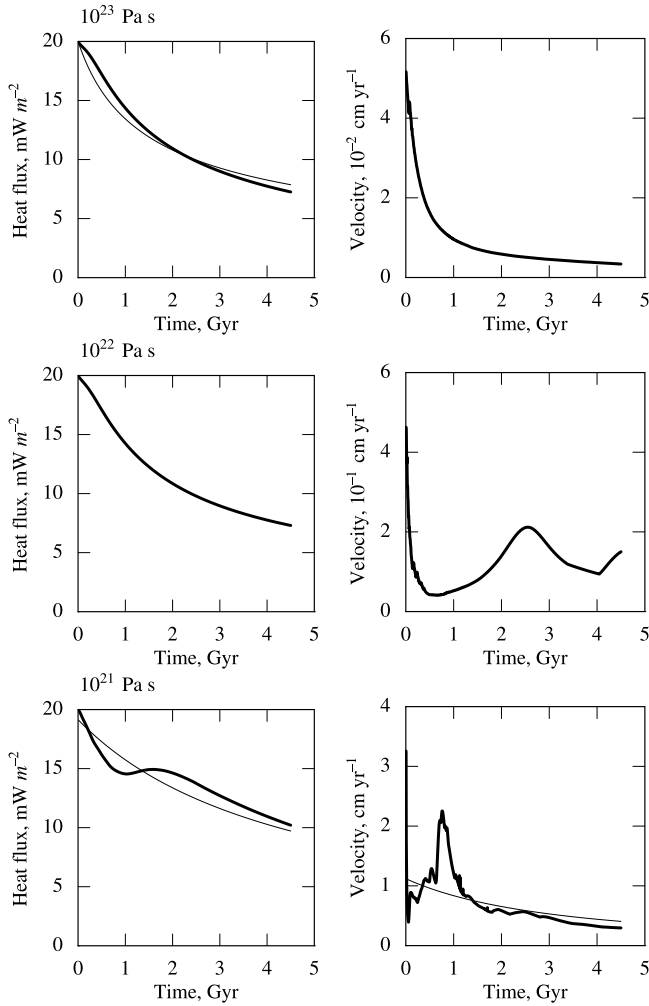


**Figure 2.** (left) Convective mantle heat flux and (right) maximum interior velocity as a function of time for the case  $R = 800$  km (heavy lines). For the high interior viscosity case ( $\eta_i \sim 10^{23}$  Pa s), the heat flux due to conductive cooling of a half space is also shown (thin line). For the low interior viscosity case ( $\eta_i \sim 10^{21}$  Pa s), the heat flux and cold plume velocity are shown for a parameterized convection calculation based on time-dependent stagnant lid convection scaling laws (thin lines) [Solomatov and Moresi, 2000].

The mantle heat flux and velocity decay with time as the spherical shell cools (Figures 2 and 3).

[28] Initial, localized upwelling results in decompression melting and associated additional depletion/melt retention buoyancy which drives an extended period of magmatism. The duration of this magmatic episode depends on interior mantle viscosity. Mantle which has undergone melting spreads out at the bottom of the viscous lid. For all cases, melt production decays with time from an initial maximum to very low levels. As interior viscosity decreases, the decay rate and total melt volume decrease and increase, respectively.

[29] The surface distribution of volcanism is directly related to the radially integrated melt fraction. Since magma transport to the surface in the stagnant lid regime is poorly

understood, no attempt is made to discriminate between intrusive and extrusive flux. Instead, the total melt volume per unit surface area (crustal thickness if all melt contributes to crustal growth) is calculated. In all cases, widespread volcanism is suppressed by lid thickening, and volcanism is concentrated in the impact plume region. For low interior viscosities, there are two spatial scales in the distribution. The outer scale is that of the impact plume. The inner scale is associated with localized, small scale convection within the plume (Figures 4 and 5). Absence of lateral melt transport at the surface leads to large amplitudes for the small scale features in the distribution. In the crustal thickness plots (Figures 4 and 5, central panel), the signal saturates at the upper end of the color scale. For the large impactor case (Figure 5), concentration of melt production in a broad ring is associated with an initial toroidal convection roll at the boundary of the hemispherical anomaly region.

#### 4. Discussion

[30] Mars Global Surveyor (MGS) topography [Smith *et al.*, 1999] plus material contained within a depression due to Tharsis loading and lithospheric flexure correspond to

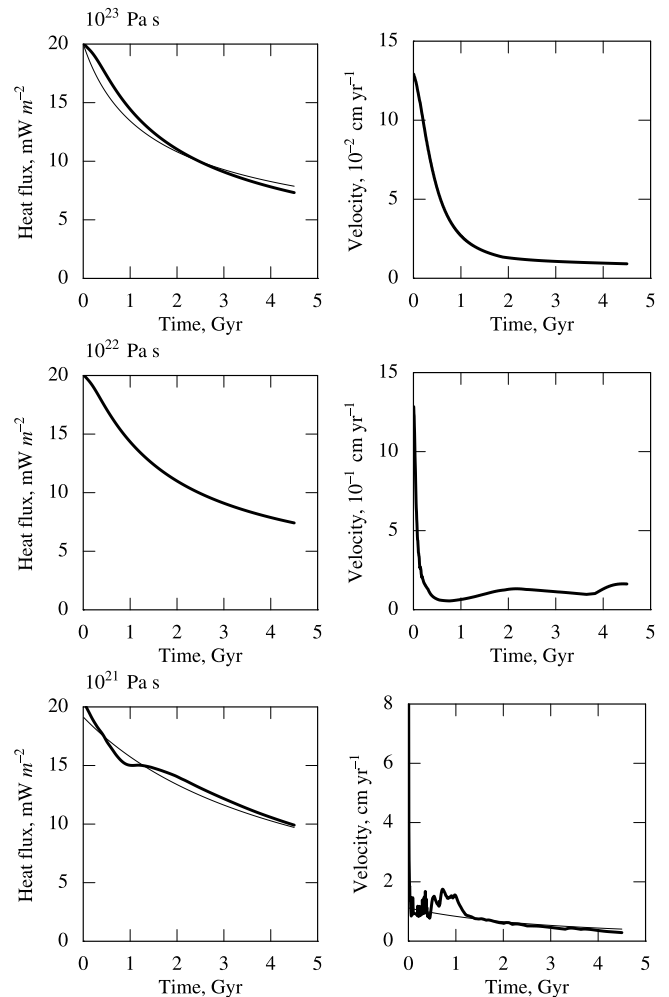


**Figure 3.** Same as Figure 2 for  $R = 1500$  km.

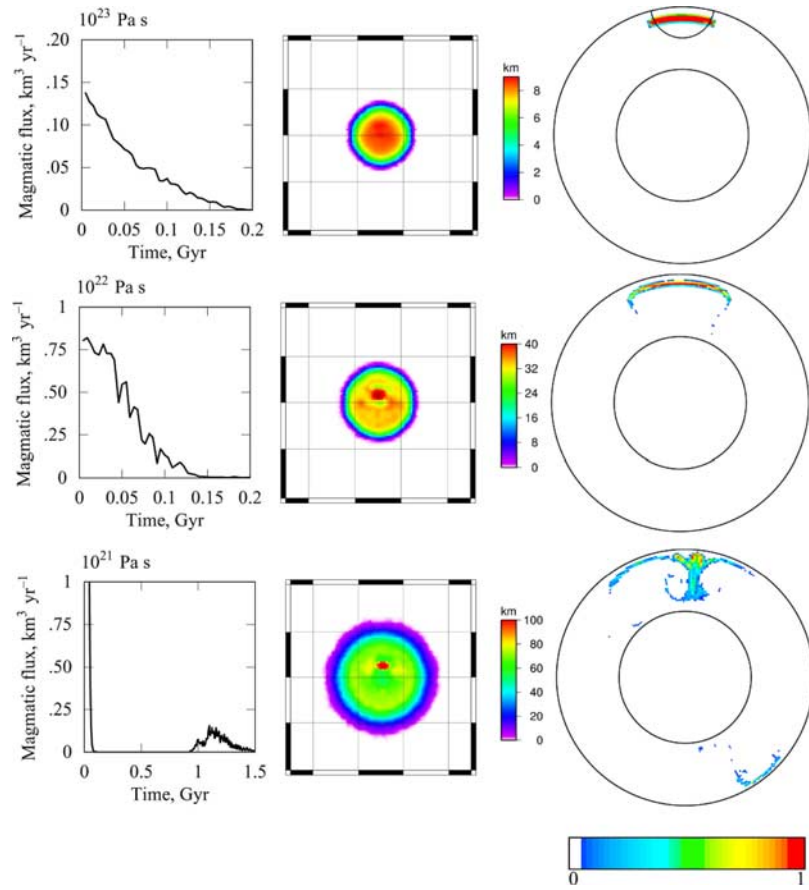


**Figure 4.** Magmatic evolution of impact plume for the case  $R = 800$  km. (left) Magmatic rate as a function of time. (middle) Final spatial distribution of the melt volume per unit surface area. The grid line and frame interval are 15. (right) Final distribution of mantle which has undergone partial melting along a cross section passing through the impact plume axis. Color (white through red) indicates volume fraction of material which has undergone partial melting, i.e., the field  $\xi$  in equation (11), and the solid line indicates the initial radius of the hemispherical anomaly.

$\sim 3 \times 10^8$  km<sup>3</sup> of igneous material [Phillips *et al.*, 2001]. For an impact plume to generate such a volcanic province, the melt production must be sufficient to obliterate the initial crater and supply material corresponding to the observed crustal load. It is well known that the melt volume generated by sufficiently large impacts can equal the crater volume [Melosh, 1989]. The impact plume mechanism proposed here suggests that even smaller impacts may be capable of erasing all evidence of the initial crater and perhaps result in the development of a large volcanic province. Using existing scaling relationships, the melt volume associated with the initial impact can be compared to the melt volume produced by the upwelling impact plume.

[31] To estimate the initial shock melting volume, the impactor radius and velocity must be specified. Clearly, the impactor size is related to the size of the hemispherical anomaly in the model. It should be emphasized, however, that the starting condition for the mantle convection simulation represents an intermediate stage of evolution after the impact and subsequent to the fast initial crystallization which results in a partially molten upper mantle and subsolidus lower mantle (see section 2.1). While the uniform temperature increase of 300 K within the anomaly region is

admittedly a simplification, the model is not sensitive to this parameter as upper mantle temperatures are dropped to the melting curve. A fully fluid dynamical simulation from impact to solid state convection is beyond the scope of this work. Instead, a scaling factor relating impactor and anomaly sizes is calculated as follows.

[32] It is assumed that the hemispherical anomaly region considered in the model represents material which underwent shock melting to at least the critical melt fraction 40% (corresponding to a rheological transition from a low viscosity crystal suspension to partially molten solid). The shock pressure corresponding to this melt fraction can be calculated from the near solidus dunite Hugoniot in pressure-entropy space [see Tonks and Melosh, 1993, Figure 4b] along with the assumption that melt fraction scales linearly with entropy, i.e.,

$$\phi = \frac{S - 2485 \text{ J/kgK}}{750 \text{ J/kgK}}. \quad (13)$$

The critical melt fraction corresponds to an entropy of 2785 J/kg K and thus a shock pressure of  $\sim 70$  GPa.

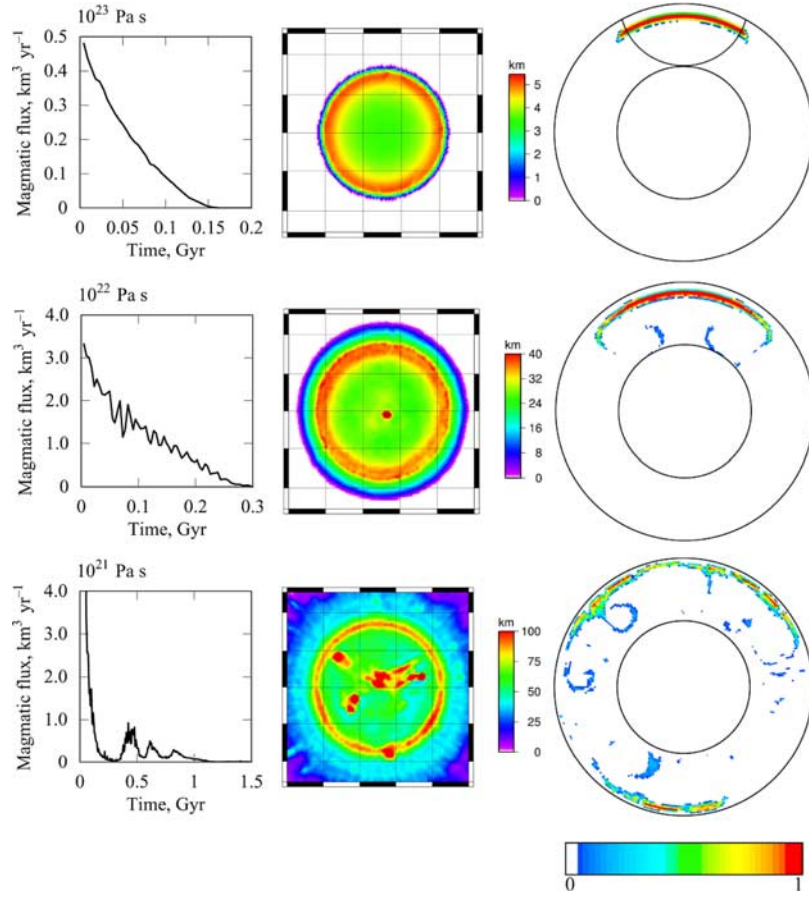


**Figure 5.** Same as Figure 4 for  $R = 1500$  km.

Adopting the notation of *Tonks and Melosh* [1993], the radius of the region shocked to pressure  $P$  or higher is

$$r = 2^{1/3} a \left( \frac{v_i}{v_i^m} \right)^{1/2}, \quad (14)$$

where  $a$  is the impactor radius,  $v_i$  is the impactor velocity, and

$$v_i^m = \frac{C}{S} \left[ \left( 1 + \frac{4SP}{\rho C^2} \right)^{1/2} - 1 \right], \quad (15)$$

where  $C$  and  $S$  are material parameters. For dunite at shock pressures  $P \geq 73$  GPa,  $C = 4.4$  km/s,  $S = 1.5$  [Kieffer, 1977]. With  $P = 70$  GPa,  $v_i^m = 4.6$  km/s and thus for  $v_i \sim 8$  km/s (mean approach velocity of

$\sim 6.5$  km/s), the anomaly radius to impactor radius ratio is  $R/a \sim 1.7$ .

[33] The ratio of the radius of the complete melt region (i.e.,  $P = 115$  GPa,  $v_i^m = 7$  km/s) to the impactor radius  $r_m/a \sim 1.3$ . The corresponding retained (outside excavation flow) melt volume

$$V_m \approx 10^6 \text{ km}^3 \left( \frac{a}{100 \text{ km}} \right)^{3.22}, \quad (16)$$

where the pi-scaling result for crater radius [Schmidt and Housen, 1987; Melosh, 1989] has been utilized, i.e.,

$$r_c \approx 300 \text{ km} \left( \frac{a}{100 \text{ km}} \right)^{0.78}. \quad (17)$$

This estimate for  $V_m$  should be considered a lower bound because partially molten regions can contribute significantly

**Table 2.** Model Results

Model Variable	Symbol (Units)	Value 1			Value 2		
Anomaly radius	$R$ (km)	800			1500		
Impactor radius	$a$ (km)	470			880		
Transient crater radius	$r_c$ (km)	1000			1600		
Complete melt radius	$r_m$ (km)	610			1100		
Crater volume	$V_c$ ( $10^8 \text{ km}^3$ )	3.8			17		
Retained impact melt volume	$V_m$ ( $10^8 \text{ km}^3$ )	1.5			11		
Interior viscosity	$\eta_i$ (Pa s)	$10^{23}$	$10^{22}$	$10^{21}$	$10^{23}$	$10^{22}$	$10^{21}$
Melting duration	$t_{melt}$ (Gyr)	0.1	0.1	0.1	0.1	0.3	1
Decompression melt volume	$V_{melt}$ ( $10^8 \text{ km}^3$ )	0.084	0.50	1.9	0.26	3.1	9.8

to the total melt volume [Tonks and Melosh, 1993]. The crater volume

$$V_c \approx 10^7 \text{ km}^3 \left( \frac{a}{100 \text{ km}} \right)^{2.35}. \quad (18)$$

[34] For Mars,  $V_m = V_c$  when  $a \sim 1400$  km and  $r_c \sim 2400$  km. For smaller impactors, the retained melt volume remaining after crystallization is extruded onto the surface during initial isostatic adjustment. After further crystallization and cooling, the evolution is controlled by solid state convection and subsequent melting is due to upwelling material intersecting the solidus from below. For the low interior viscosity ( $\eta_i \sim 10^{21}$  Pa s) cases, the melt volume produced via decompression melting associated with the upwelling impact plume is of the order of the initial retained melt volume (Table 2). It seems likely that, in these cases, the impact plume mechanism can contribute significantly to the total extrusive melt volume. Perhaps a large impactor, via extrusion of initial shock melt and impact-plume decompression melting, has the potential to result in development of a large volcanic construct.

[35] While magma transport and crustal development in the stagnant lid regime is poorly understood, the gross features of the model melt distribution can be compared to the present day observations of crustal thickness. MGS topography and gravity indicate a complex crust within Tharsis province characterized by variable thickening superimposed on the global south-north trend [Zuber et al., 2000; Zuber, 2001]. A single large impact plume beneath Tharsis is consistent with a monopolar surface volcanism distribution and crustal thickening within the plateau similar to a conventional thermal plume [e.g., Harder and Christensen, 1996]. In southern Tharsis province, Solis Planum exhibits regionally thicker crust corresponding to enhanced melting [Zuber et al., 2000; Zuber, 2001]. The low interior viscosity cases predict small scale convection within the impact plume (similar to instabilities which develop during thermal plume-lithosphere interaction [Moore et al., 1999]) and associated localized melting. There is no present day observation suggestive of circumferential concentration of melt production (Figure 5) around Tharsis. The duration of large scale impact plume melting for all cases is  $<1$  Gyr which is approximately the time by which Tharsis was emplaced [Banerdt and Golombek, 2000; Phillips et al., 2001; Johnson and Phillips, 2003; Zuber, 2001].

## 5. Conclusions

[36] 1. Impact-induced thermochemical plumes can play an important role in mantle dynamics and Martian evolution. Compositional buoyancy associated with impact heating, melting, and differentiation can pin mantle upwellings and focus subsequent magmatic activity.

[37] 2. For sufficiently low interior viscosity, impact plume decompression melt volumes are on the order of initial retained shock melt volumes. In this case, a sufficiently large impact has the potential to obliterate the initial crater and result in development of a large igneous province. Large scale melting ceases by the end of the Noachian consistent with timing of Tharsis formation.

[38] 3. The initial thermal and compositional state of the Martian mantle is an outstanding problem. Clearly the preimpact spherical symmetry assumed in this study is a zero order approximation. Prior to the last impacts, mantle temperature and composition is affected by earlier impacts, core formation, and previous mantle dynamics. This can be addressed within the context of the model by prescribing a plausible impactor mass spectrum or specifying thermal and compositional heterogeneity in a statistical fashion.

[39] **Acknowledgments.** The authors thank H. J. Melosh for constructive reviews which greatly benefited the paper. This work was supported by NASA grants NAG5-8803 and NAG5-13123 and the New Mexico Universities Collaborative Research Program. Convection simulations were performed on the NMSU Geodynamics Beowulf cluster Muromets. Funding for the cluster was provided by NSF grant EAR-02-7495.

## References

- Agnor, C. B., R. M. Canup, and H. F. Levison (1999), On the character and consequences of large impacts in the late stage of terrestrial planet formation, *Icarus*, *142*, 219–237.
- Albarède, F., J. Blichert-Toft, J. D. Vervoort, J. D. Gleason, and M. Rosing (2000), Hf-Nd isotope evidence for a transient dynamic regime in the early terrestrial mantle, *Nature*, *404*, 488–490.
- Avé Lallemand, H. G. (1978), Experimental deformation of diopside and websterite, *Tectonophysics*, *48*, 1–27.
- Banerdt, W. B., and M. P. Golombek (2000), Tectonics of the Tharsis region of Mars: Insights from MGS topography and gravity, *Proc. Lunar Planet. Sci. Conf. 31st*, abstract 2038.
- Baumgardner, J. R. (1985), Three dimensional treatment of convective flow in the Earth's mantle, *J. Stat. Phys.*, *39*, 501–511.
- Bertka, C. M., and Y. W. Fei (1998a), Density profile of an SNC model Martian interior and the moment of inertia factor of Mars, *Earth Planet. Sci. Lett.*, *157*, 79–88.
- Bertka, C. M., and Y. W. Fei (1998b), Implication of Mars Pathfinder data for the accretion history of the terrestrial planets, *Science*, *281*, 1838–1840.
- Bertka, C. M., and Y. W. Fei (1999), Geophysical and geochemical constraints on the composition and structure of the Martian interior, in *5th International Conference on Mars, LPI Contrib. 972*, abstract 6225, Lunar and Planet. Inst., Houston, Tex.
- Breuer, D., D. A. Yuen, T. Spohn, and S. Zhang (1998), Three dimensional models of Martian mantle convection with phase transitions, *Geophys. Res. Lett.*, *25*, 229–232.
- Bunge, H.-P., and J. R. Baumgardner (1995), Mantle convection modeling on parallel virtual machines, *Comput. Phys.*, *9*, 207–215.
- Carr, M. H. (1974), Tectonism and volcanism of the Tharsis region of Mars, *J. Geophys. Res.*, *79*, 3943–3949.
- Chambers, J. E., and G. W. Wetherill (1998), Making the terrestrial planets: N-body integrations of planetary embryos in three dimensions, *Icarus*, *136*, 304–327.
- Dullien, F. A. L. (1979), *Porous Media: Fluid Transport and Pore Structure*, Academic, San Diego, Calif.
- Dumoulin, C., M.-P. Doin, and L. Fleitout (1999), Heat transport in stagnant lid convection with temperature and pressure dependent Newtonian or non-Newtonian rheology, *J. Geophys. Res.*, *104*, 12,759–12,777.
- Elkins-Tanton, L. T., B. H. Hager, and T. L. Grove (2002), Magmatic effects of the lunar late heavy bombardment, *Proc. Lunar Planet. Sci. Conf. 33rd*, abstract 1422.
- Grasset, O., and E. M. Parmentier (1998), Thermal convection in a volumetrically heated, infinite Prandtl number fluid with strongly temperature-dependent viscosity: Implications for planetary thermal evolution, *J. Geophys. Res.*, *103*, 18,171–18,181.
- Halliday, A. N., H. Wänke, J.-L. Birck, and R. N. Clayton (2001), The accretion, composition, and early differentiation of Mars, *Earth Moon Planets*, *96*, 197–230.
- Harder, H. (2000), Mantle convection and the dynamic geoid of Mars, *Geophys. Res. Lett.*, *27*, 301–304.
- Harder, H., and U. R. Christensen (1996), A one-plume model of Martian mantle convection, *Nature*, *380*, 507–509.
- Harper, C. L., L. E. Nyquist, B. Bensch, H. Wiesmann, and C.-Y. Shih (1995), Rapid accretion and early differentiation of Mars indicated by  $^{142}\text{Nd}/^{144}\text{Nd}$  in SNC meteorites, *Science*, *267*, 213–217.

- Hartmann, W. K. (1973), Martian surface and crust: Review and synthesis, *Icarus*, *19*, 550–575.
- Hauck, S. A., II, and R. J. Phillips (2002), Thermal and crustal evolution of Mars, *J. Geophys. Res.*, *107*(E7), 5052, doi:10.1029/2001JE001801.
- Herzberg, C., and J. Z. Zhang (1994), Melting experiments on anhydrous peridotite KLB-1 from 5.0 to 22.5 Gpa, *J. Geophys. Res.*, *99*, 17,729–17,742.
- Hess, P. C. (1992), Phase equilibria constraints on the origin of ocean floor basalts, in *Mantle Flow and Melt Generation at Mid-Ocean Ridges*, *Geophys. Monogr. Ser.*, vol. 71, edited by J. Phipps Morgan, D. K. Blackman, and J. M. Sinton, pp. 67–102, AGU, Washington, D.C.
- Ito, E., and E. Takahashi (1987), Melting of peridotite at uppermost lower-mantle conditions, *Nature*, *328*, 514–517.
- Johnson, C. L., and R. J. Phillips (2003), Constraints on the evolution of the Tharsis region of Mars, *Proc. Lunar Planet. Sci. Conf. 33rd*, abstract 1360.
- Jones, A. P., G. D. Price, N. J. Price, P. S. DeCarli, and R. A. Clegg (2002), Impact induced melting and the development of large igneous provinces, *Earth Planet. Sci. Lett.*, *202*, 551–561.
- Karato, S.-I. (1986), Does partial melting reduce the creep strength of the upper mantle?, *Nature*, *319*, 8151–8176.
- Karato, S.-I., and P. Wu (1993), Rheology of the upper mantle: A synthesis, *Science*, *260*, 771–778.
- Kieffer, S. W. (1977), Impact conditions required for formation of melt by jetting in silicates, in *Impact and Explosion Cratering*, edited by D. J. Roddy, R. O. Pepin, and R. B. Merrill, Pergamon, New York.
- Kushiro, I. (1980), Viscosity, density, and structure of silicate melts at high pressures, and their petrological applications, in *Physics of Magmatic Processes*, edited by R. B. Hargraves, Princeton Univ. Press, Princeton, N. J.
- Kushiro, I. (1986), Viscosity of partial melts in the upper mantle, *J. Geophys. Res.*, *91*, 9343–9350.
- Lee, D. C., and A. N. Halliday (1997), Core formation on Mars and differentiated asteroids, *Nature*, *388*, 854–857.
- Lowry, A. R., and S. Zhong (2003), Surface versus internal loading of the Tharsis rise, Mars, *J. Geophys. Res.*, *108*(E9), 5099, doi:10.1029/2003JE002111.
- Mackwell, S. J. (1991), High temperature rheology of enstatite: Implications for creep in the mantle, *Geophys. Res. Lett.*, *18*, 2027–2030.
- Marty, B., and K. Marti (2002), Signatures of early differentiation of Mars, *Earth Planet. Sci. Lett.*, *196*, 251–263.
- McEwen, A. S., M. C. Malin, M. H. Carr, and W. K. Hartmann (1999), Voluminous volcanism on early Mars revealed in Valles Marineris, *Nature*, *397*, 584–586.
- McKenzie, D., and M. J. Bickle (1988), The volume and composition of melt generated by extension of the lithosphere, *J. Petrol.*, *29*, 625–679.
- McKenzie, D., and M. J. Bickle (1990), A eutectic parameterization of mantle melting, *J. Phys. Earth*, *38*, 511–515.
- McLennan, S. M. (2001), Crustal heat production and the thermal evolution of Mars, *Geophys. Res. Lett.*, *28*, 4019–4022.
- Melosh, H. J. (1989), *Impact Cratering: A Geological Process*, Oxford Univ. Press, New York.
- Melosh, H. J. (1990), Giant impacts and thermal state of the early Earth, in *Origin of the Earth*, edited by H. E. Newsom and J. H. Jones, Oxford Univ. Press, New York.
- Melosh, H. J. (2000), Can impacts induce volcanic eruptions?, paper presented at Catastrophic Events and Mass Extinctions: Impacts and Beyond, Univ. of Vienna, Vienna.
- Moore, W. B., G. Schubert, and P. J. Tackley (1999), The role of rheology in lithospheric thinning by mantle plumes, *Geophys. Res. Lett.*, *26*, 1073–1076.
- Nimmo, F., and D. Stevenson (2000), The influence of early plate tectonics on the thermal evolution and magnetic field of Mars, *J. Geophys. Res.*, *105*, 11,969–11,979.
- Oxburgh, E. R., and E. M. Parmentier (1977), Compositional and density stratification in oceanic lithosphere: Causes and consequences, *J. Geol. Soc. London*, *133*, 343–355.
- Pierazzo, E., and H. J. Melosh (2000), Melt production in oblique impacts, *Icarus*, *145*, 252–261.
- Pierazzo, E., A. M. Vickery, and H. J. Melosh (1997), A reevaluation of impact melt production, *Icarus*, *127*, 408–423.
- Phillips, R. J., and E. R. Ivins (1979), Geophysical observations pertaining to solid-state convection in the terrestrial planets, *Phys. Earth Planet. Inter.*, *19*, 107–148.
- Phillips, R. J., N. H. Sleep, and W. B. Banerdt (1990), Permanent uplift in magmatic systems with application to the Tharsis region of Mars, *J. Geophys. Res.*, *95*, 5089–5100.
- Phillips, R. J., et al. (2001), Ancient geodynamics and global scale hydrology on Mars, *Science*, *291*, 2587–2591.
- Raddick, M. J., E. M. Parmentier, and D. S. Scheirer (2002), Buoyant decompression melting: A possible mechanism for intraplate volcanism, *J. Geophys. Res.*, *107*(B10), 2228, doi:10.1029/2001JB000617.
- Reese, C. C., V. S. Solomatov, and L.-N. Moresi (1998), Heat transport efficiency for stagnant lid convection with dislocation viscosity: Application to Mars and Venus, *J. Geophys. Res.*, *103*, 13,643–13,657.
- Reese, C. C., V. S. Solomatov, and L.-N. Moresi (1999a), Non-Newtonian stagnant lid convection and magmatic resurfacing on Venus, *Icarus*, *139*, 67–80.
- Reese, C. C., V. S. Solomatov, J. R. Baumgardner, and W.-S. Wang (1999b), Stagnant lid convection in a spherical shell, *Phys. Earth Planet. Inter.*, *116*, 1–7.
- Reese, C. C., V. S. Solomatov, and J. R. Baumgardner (2002), Survival of impact-induced thermal anomalies in the Martian mantle, *J. Geophys. Res.*, *107*(E10), 5082, doi:10.1029/2000JE001474.
- Ross, J. V., and K. C. Nielsen (1978), High temperature flow of wet polycrystalline enstatite, *Tectonophysics*, *44*, 233–261.
- Sanloup, C., A. Jambon, and P. Gillet (1999), A simple chondritic model of Mars, *Phys. Earth Planet. Inter.*, *112*, 43–54.
- Scarfe, C. M., and E. Takahashi (1986), Melting of garnet peridotite to 13 GPa and the early history of the upper mantle, *Nature*, *322*, 354–356.
- Schmidt, R. M., and K. R. Housen (1987), Some recent advances in the scaling of impact and explosion cratering, *Int. J. Impact Eng.*, *5*, 543–560.
- Schubert, G., S. C. Solomon, D. L. Turcotte, M. J. Drake, and N. H. Sleep (1992), Origin and thermal evolution of Mars, in *Mars*, edited by H. H. Kieffer et al., pp. 147–183, Univ. of Ariz. Press, Tucson.
- Schultz, P. H. (1984), Impact basin control of volcanic and tectonic provinces on Mars, *Proc. Lunar Planet. Sci. Conf. 15th*, Part 1, *J. Geophys. Res.*, *89*, suppl., 728–729.
- Schultz, R. A., and H. V. Frey (1990), A new survey of large multiring impact basins on Mars, *J. Geophys. Res.*, *95*, 14,175–14,189.
- Schultz, P. H., and H. Glicken (1979), Impact crater and basin control of igneous processes on Mars, *J. Geophys. Res.*, *84*, 8033–8047.
- Sleep, N. H. (1994), Martian plate tectonics, *J. Geophys. Res.*, *99*, 5639–5655.
- Smith, D. E., et al. (1999), The global topography of Mars and implications for surface evolution, *Science*, *284*, 1495–1503.
- Solomatov, V. S. (2000), Fluid dynamics of magma oceans, in *Origin of the Earth and Moon*, edited by R. Canup and K. Righter, pp. 323–338, Univ. of Ariz. Press, Tucson.
- Solomatov, V. S., and L.-N. Moresi (2000), Time dependent stagnant lid convection on the Earth and other terrestrial planets, *J. Geophys. Res.*, *105*, 21,795–21,817.
- Solomon, S. C., and J. W. Head (1982), Evolution of the Tharsis province of Mars: The importance of heterogeneous lithospheric thickness and volcanic construction, *J. Geophys. Res.*, *87*, 9755–9774.
- Soo, S. H. (1967), *Fluid Dynamics of Multiphase Systems*, 524 pp., Blaisdell, Waltham, Mass.
- Sparks, D. W., and E. M. Parmentier (1993), The structure of three-dimensional convection beneath oceanic spreading centres, *Geophys. J. Int.*, *112*, 81–91.
- Spohn, T. (1991), Mantle differentiation and thermal evolution of Mars, Mercury, and Venus, *Icarus*, *90*, 222–236.
- Spohn, T., F. Sohl, and D. Breuer (1998), Mars, *Astron. Astrophys. Rev.*, *8*, 181–235.
- Tajika, E., and S. Sasaki (1996), Magma generation on Mars constrained from <sup>40</sup>Ar degassing model, *J. Geophys. Res.*, *101*, 7543–7554.
- Tonks, W. B., and H. J. Melosh (1992), Core formation by giant impacts, *Icarus*, *100*, 326–346.
- Tonks, W. B., and H. J. Melosh (1993), Magma ocean formation due to giant impacts, *J. Geophys. Res.*, *98*, 5319–5333.
- Turcotte, D. L. (1989), Thermal evolution of Mars and Venus including irreversible fractionation, *Proc. Lunar Planet. Sci. Conf. 20th*, 1138–1139.
- Turcotte, D. L., and G. Schubert (2002), *Geodynamics*, Cambridge Univ. Press, New York.
- Warner, N. H., and T. K. P. Gregg (2003), Evolved lavas on Mars? Observations from southwest Arsia Mons and Sabancaya volcano, Peru, *J. Geophys. Res.*, *108*(E10), 5112, doi:10.1029/2002JE001969.
- Weidenschilling, S. J., D. Spaute, D. R. Davis, F. Marzari, and K. Ohtsuki (1997), Accretional evolution of a planetesimal swarm. 2. The terrestrial zone, *Icarus*, *126*, 429–455.
- Weinstein, S. A. (1995), The effects of a deep mantle endothermic phase change on the structure of thermal convection in silicate planets, *J. Geophys. Res.*, *100*, 11,719–11,728.

- Wetherill, G. W. (1985), Occurrence of giant impacts during the growth of the terrestrial planets, *Science*, *228*, 877–879.
- Wetherill, G. W. (1990), Formation of the Earth, *Annu. Rev. Earth Planet. Sci.*, *18*, 205–256.
- Yoder, C. F., A. S. Konopliv, D. N. Yuan, E. M. Standish, and W. M. Folkner (2003), Fluid core size of Mars from detection of the Solar tide, *Science*, *300*, 299–303.
- Zhong, S. (2002), Effects of lithosphere on the long-wavelength gravity anomalies and their implications for the formation of the Tharsis rise on Mars, *J. Geophys. Res.*, *107*(E7), 5054, doi:10.1029/2001JE001589.
- Zhong, S., and J. H. Roberts (2003), On the support of the Tharsis Rise on Mars, *Earth Planet. Sci. Lett.*, *214*, 1–9.
- Zuber, M. T. (2001), The crust and mantle of Mars, *Nature*, *412*, 220–227.
- Zuber, M. T., et al. (2000), Internal structure and early thermal evolution of Mars from Mars Global Surveyor topography and gravity, *Science*, *287*, 1788–1793.
- 
- J. R. Baumgardner, Theoretical Division, Los Alamos National Laboratory, MS B216, Los Alamos, NM 87545, USA. (johnrb@lanl.gov)
- C. C. Reese, Division of Science and Mathematics, University of Minnesota, Morris, Morris, MN 56267, USA. (resec@mrs.umn.edu)
- V. S. Solomatov and A. V. Veolainen, Department of Physics, New Mexico State University, Las Cruces, NM 88003, USA. (slava@nmsu.edu; a\_vez@nmsu.edu)
- D. R. Stegman, Department of Earth and Planetary Science, University of California, Berkeley, CA 94720, USA. (dstegman@eps.berkeley.edu)